Electronic Supplementary Material (ESI) for Physical Chemistry Chemical Physics.

Supplementary data for

Donor Engineering of a Benzothiadiazole-Based D-A-D-type Molecular Semiconductor for Perovskite Solar Cells: A Theoretical Study

Zhu-Zhu Sun,* Yushan Li,* and Xing-Lei Xu

College of Physics and Electronic Engineering, Heze University, Heze 274015, China

E-mail: Z.Z.Sun: sunzhuzhu@hezeu.edu.cn; Y.Li: lysh507@163.com

Computational methods

1.1 Theoretical background

The hole-transporting ability of HTMs in this work is evaluated by the Marcus theory of electron transfer coupled with the Einstein relation,[1]

$$\mu = \frac{eD}{k_B T}$$

where e is the electron charge, and D is the charge diffusion coefficient, k_B is the Boltzmann's constant, and T is the temperature in Kelvin.

For isotropic systems, the diffusion coefficient D can be expressed as

$$D = \frac{1}{2d}\sum_i r_i^2 k_i p_i$$

where i represents a given hole hopping channel, r_i denotes the centroid to centroid distance, d is the spatial dimensionality, and taken as 3 due to the charge diffusion is considered in three dimensions, and p_i ($p_i = k_i \Big/ \sum_i k_i$) is the hopping probability for the *i*-th channel.

Due to the weak transfer integral in organic semiconductor, the hole hopping rate (κ) is calculated by the semi-classical Marcus theory,[2]

$$\kappa = \frac{2\pi}{\hbar} V_{ab}^2 \frac{1}{\sqrt{4\pi\lambda k_B T}} exp\left[-\lambda / 4k_B T \right]$$

where V_{ab} is the hole transfer integral, λ denotes hole reorganization energy, and $\hbar$ is the Planck's constant. Herein, the reorganization energy is gained by the adiabatic potential energy surface method,[3] and hole transfer integral is calculated with a direct coupling method.[4]

$$V_{ab} = \left\langle \psi_{HOMO}^{0,a} \middle| F \middle| \psi_{HOMO}^{0,b} \right\rangle$$

where $\psi_{HOMO}^{0,a}$ and $\psi_{HOMO}^{0,b}$ are the HOMOs of two adjacent molecules *a* and *b* with no intermolecular interaction is present, and F is the Fock operator. The hole transfer integral is calculated by the functional PW91PW91 and the 6-31G** basis set.[5-8]

The orbital overlapping integrals between adjacent molecules are calculated with the following formula,

$$S_{i,j}^{intmol} = \int \varphi_{i}^{monomer1}(r)\varphi_{j}^{monomer2}(r)dr$$

where *i*, *j* are molecular orbital indices of monomer 1 and monomer 2, respectively.

1.2 Computational details

As reported in previous works,[9-10] the BMK functional and the 6-31G** basis set can provide the relatively accurate description of neutral geometries of HTMs. Meanwhile, the accurate estimations of the electronic and optical properties of HTMs can also be presented. Therefore, both the ground-state (S_0) and first excited-state (S_1) geometric structures of investigated HTMs are optimized at the BMK/6-31G** level. To further probe the functional effect on geometry optimization, the B3LYP/6-31G** method is also performed. The results indicate that the HOMO levels of investigated HTMs are extremely underestimated by the B3LYP/6-31G** method compared with that of the BMK/6-31G** method though the more stable geometries are obtained by the B3LYP functional. Therefore, we believe that the direct calculation from the B3LYP/6-31G** method is not suitable for this work. The same trend for the HOMOs and the LUMOs can be gained by the two methods, as provided in the Table S2. The dichloromethane coupled with the C-PCM model are employed to simulate the solvent effects.[11] Based

on the optimized S_0 geometries, the optical absorption spectra of HTMs are simulated by the time-dependent DFT (TD-DFT) method at the same theoretical level. Herein, the lowest 50 singlet-singlet excited states were considered for the vertical transitions. Meantime, the emission wavelengths and the intramolecular charge transfer properties are calculated on the basis of the ground-geometries. The absorption spectra of HTMs are plotted with the Multiwfn 3.7 program,[12] and the full width at half maximum is set to 0.67 eV. To evaluate the intramolecular charge transfer properties during the optical excitation, the charge transfer amounts (q_{CT}) and distances (d_{CT}) are calculated using the method reported by Ciofini et al.[13-14] The charge transfer properties are evaluated at the BMK/6-31G** level to remain the consistency with the vertical absorption, and the charge density difference (CDD) maps are plotted by the Multiwfn 3.7 program.[12] According to the previous reports,[15-20] the Gibbs solvation free energies are calculated with the M05-2X/6-31G** method, coupled with SMD model. The molecular orbital composition analysis for the HOMOs is carried out with the Multiwfn 3.7 program,[12] The above DFT and TD-DFT calculations are performed by Gaussian 09 packge.[21]

In order to calculate the transfer integral and the corresponding hopping rate, the crystal structures of studied HTMs are necessary. In this work, the crystal predictions are carried out with the polymorph in Materials Studio,[22] and the detailed calculation procedures are given in our previous works.[7-8,10] The five most probable space groups, $P21/C$, $P1$, $P212121$, $C2/C$ and $P21$ are employed for the predictions. Based on the predicted crystals, the possible dimeric structures are generated.

The PbI_2-terminated (100) surfaces of cubic $FAPbI_3$ are employed to research the adsorbed influences of HTMs.[7-8] The surfaces are composed of (3×5) supercells, and a vacuum of 25 Å is added in z direction to avoid periodic interactions. All calculations are performed by the Vienna ab initio package (VASP).[23-24] The GGA-PBE functional and the projector-augmented wave pseudopotential are used to describe the exchange and correlation interactions.[25-26] The spin polarization and an energy cutoff of 400 eV are utilized to achieve the energy and force convergence of 0.1 meV and 20 meV $Å^{-1}$, respectively. Meanwhile, the Grimme's D3 method is also considered to describe the weak van der Waals interactions.[27]

References

1. L. B. Schein and A. R. McGhie, *Phys. Rev. B*, 1979, **20**, 1631-1639.
2. R.A. Marcus and N. Sutin, *Biochim. Biophys. Acta*, 1985, **811**, 265-322.
3. Z. Z. Sun, S. Feng and W. L. Ding, *Synth. Met.*, 2020, **259**, 116219.
4. T. Fujita, H. Nakai and H. Nakatsuji, *J. Chem. Phys.*, 1996, **104**, 2410-2417.
5. Y. Zhao and D. G. Truhlar, *Theor. Chem. Acc.*, 2008, **120**, 215-241.
6. Z. Z. Sun, J. Yang, W. L. Ding, J. L. Liu and X. L. Xu, *J. Phys. Chem. C*, 2022, **126**, 11529-11536.
7. Z. Z. Sun and R. Long, *J. Phys. Chem. C*, 2023, **127**, 8953-8962.
8. Z. Z. Sun and R. Long, *J. Phys. Chem. C*, 2023, **127**, 12913-12922.
9. W. X. Hu, Z. M. Zhang, J. Y. Cui, W. Shen, M. Li and R. X. He, *Nanoscale*, 2017, **9**, 12916-12924.
10. Z. Z. Sun, S. Feng, C. Gu, N. Cheng and J. Liu, *Phys. Chem. Chem. Phys.*, 2019, **21**, 15206-15214.
11. J. Tomasi, B. Mennucci and R. Cammi, *Chem. Rev.*, 2005, **105**, 2999-3093.
12. T. Lu and F. W. Chen, *J. Comput. Chem.*, 2012, **33**, 580-592.
13. T. Le Bahers, C. Adamo and I. Ciofini, *J. Chem. Theory Comput.*, 2011, **7**, 2498-2506.
14. I. Ciofini, T. Le Bahers, C. Adamo, F. Odobel and D. Jacquemin, *J. Phys. Chem. C*, 2012, **116**, 11946-11955.
15. J. Ho, A. Klamt and M. L. Coote, *J. Phys. Chem. A*, 2010, **114**, 13442-13444.
16. A. V. Marenich, C. J. Cramer and D. G. Truhlar, *J. Phys. Chem. B*, 2009, **113**, 6378-6396.
17. R. F. Ribeiro, A. V. Marenich, C.J. Cramer and D. G. Truhlar, *J. Phys. Chem. B*, 2011, **115**, 14556-14562.

18. V. S. Bernales, A. V. Marenich, R. Contreras, C. J. Cramer and D. G. Truhlar, *J. Phys. Chem. B*, 2012, **116**, 9122-9129.
19. W. Zhu, K. Zhou, Y. Fo, Y. Li, B. Guo, X. Zhang and X. Zhou, *Phys. Chem. Chem. Phys.*, 2022, **24**, 18793-18804.
20. M. Hao, W. J. Chi and Z. S. Li, *Nanoscale*, 2021, **13**, 4241-4248.
21. M. J. Frisch, G. W. Trucks, H. B. Schlegel, G. E. Scuseria, M. A. Robb, J. R. Cheeseman, G. Scalmani, V. Barone, B. Mennucci, G. A. Petersson, H. Nakatsuji, M. Caricato, X. Li, H. P. Hratchian, A. F. Izmaylov, J. Bloino, G. Zheng, J. L. Sonnenberg, M. Hada, M. Ehara, K. Toyota, R. Fukuda, J. Hasegawa, M. Ishida, T. Nakajima, Y. Honda, O. Kitao, H. Nakai, T. Vreven, J. A. Montgomery, Jr., J. E. Peralta, F. Ogliaro, M. Bearpark, J. J. Heyd, E. Brothers, K. N. Kudin, V. N. Staroverov, R. Kobayashi, J. Normand, K. Raghavachari, A. Rendell, J. C. Burant, S. S. Iyengar, J. Tomasi, M. Cossi, N. Rega, J. M. Millam, M. Klene, J. E. Knox, J. B. Cross, V. Bakken, C. Adamo, J. Jaramillo, R. Gomperts, R. E. Stratmann, O. Yazyev, A. J. Austin, R. Cammi, C. Pomelli, J. W. Ochterski, R. L. Martin, K. Morokuma, V. G. Zakrzewski, G. A. Voth, P. Salvador, J. J. Dannenberg, S. Dapprich, A. D. Daniels, Ö. Farkas, J. B. Foresman, J. V. Ortiz, J. Cioslowski, and D. J. Fox, *Gaussian 09, Revision D.01*, Gaussian, Inc., Wallingford, CT, 2009.
22. One Molecular Simulation Software. https://www.accelrys.com.
23. G. Kresse and J. Furthmuller, *Phys. Rev. B*, 1996, **54**, 11169-11186.
24. G. Kresse and J. Furthmuller, *Comput. Mater. Sci.*, 1996, **6**, 15-50.
25. J. P. Perdew, K. Burke and M. Ernzerhof, *Phys. Rev. Lett.*, 1996, **77**, 3865-3868.
26. P. E. Blochl, *Phys. Rev. B*, 1994, **50**, 17953-17979.
27. S. Grimme, *J. Comput. Chem.*, 2006, **27**, 1787-1799.

Table S1 Orbital composition analysis of the HOMOs for SM36, SM38 and SM40.

HTMs	acceptor and spacer	donor
SM36	28.4%	35.8%
SM38	39.6%	30.2%
SM40	59.5%	20.2%

Table S2 The calculated HOMO and the LUMO levels (in eV) of investigated HTMs using the BMK/6-31G** and the B3LYP/6-31G** methods, respectively. The energy differences (ΔE, in eV) of HTMs are calculated by $\Delta E = E_{BMK} - E_{B3LYP}$.

HTMs	BMK/6-31G**		B3LYP/6-31G**		ΔE
	E_H	E_L	E_H	E_L	
SM35	-5.26	-2.02	-4.57	-2.61	39.3
SM36	-5.37	-2.15	-4.67	-2.68	44.7
SM37	-5.43	-2.04	-4.72	-2.64	44.6
SM38	-5.58	-2.17	-4.85	-2.71	50.0
SM39	-5.43	-1.98	-4.74	-2.58	37.8
SM40	-5.64	-2.10	-4.92	-2.65	43.2
YN1	-5.33	-1.72	-4.69	-2.35	43.0
YN1-T	-5.14	-1.90	-4.48	-2.48	46.7

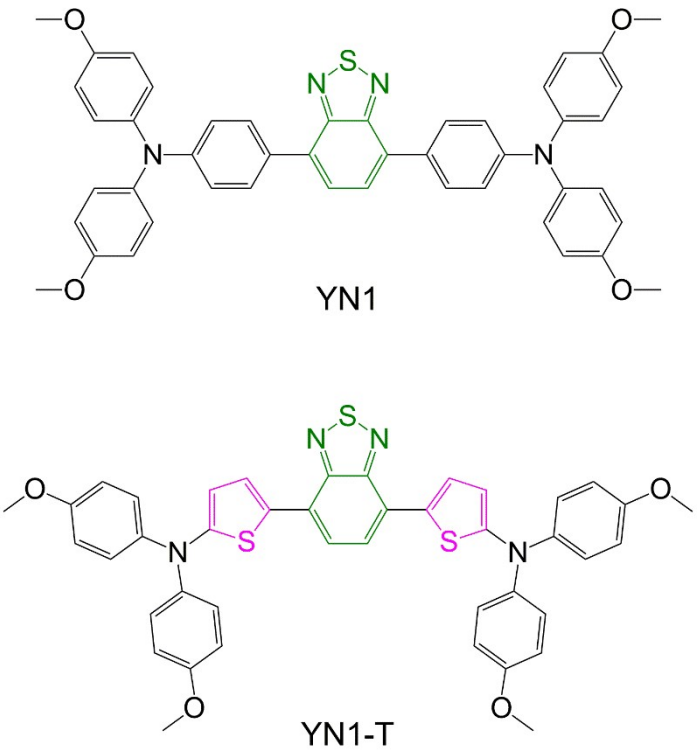

Fig. S1 Chemical structure of the YN1 and YN1-T.

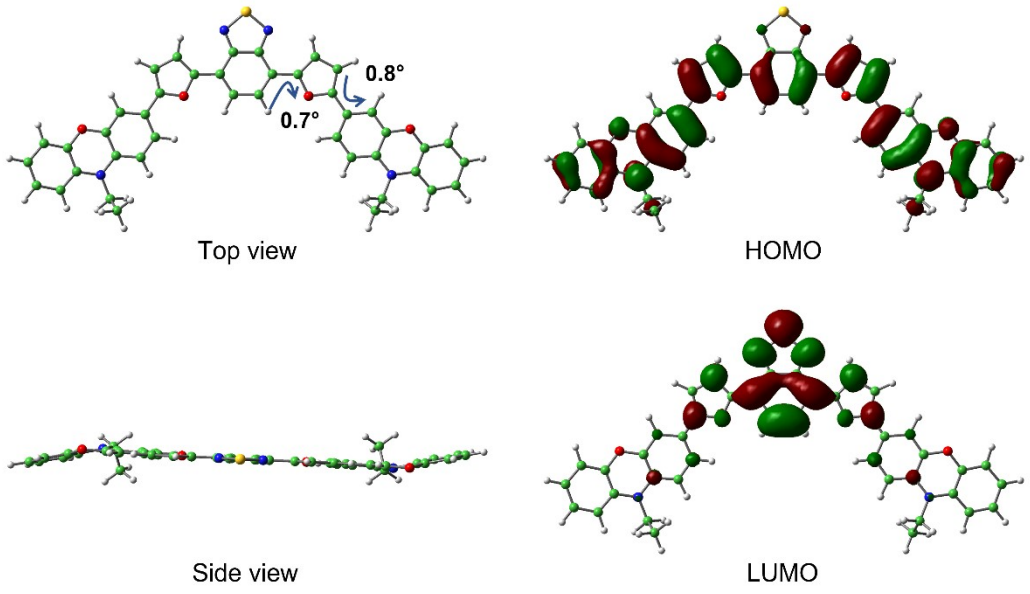

Fig. S2 Optimized structure, the HOMO and the LUMO distributions of the SM35.

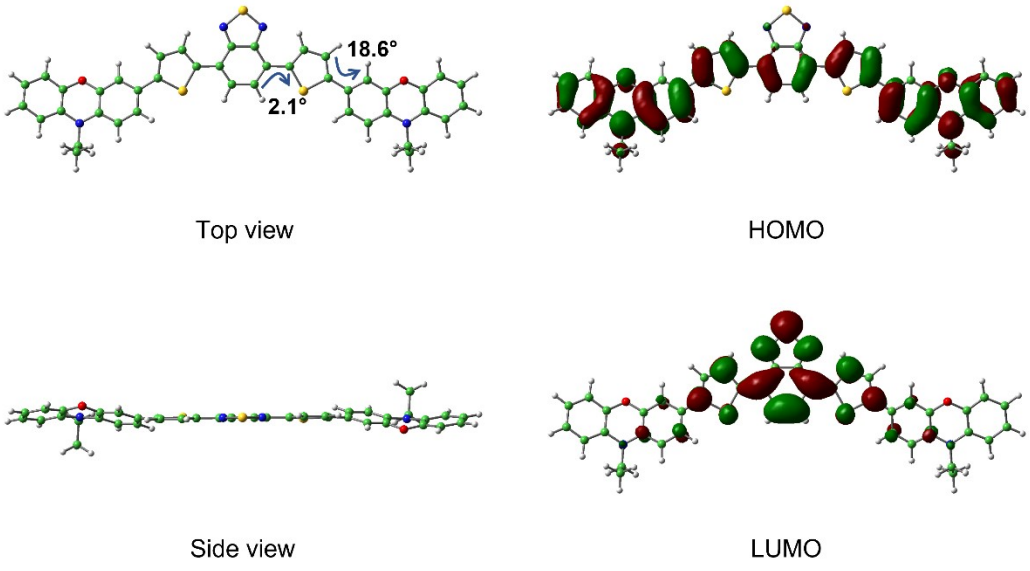

Fig. S3 Optimized structure, the HOMO and the LUMO distributions of the SM36.

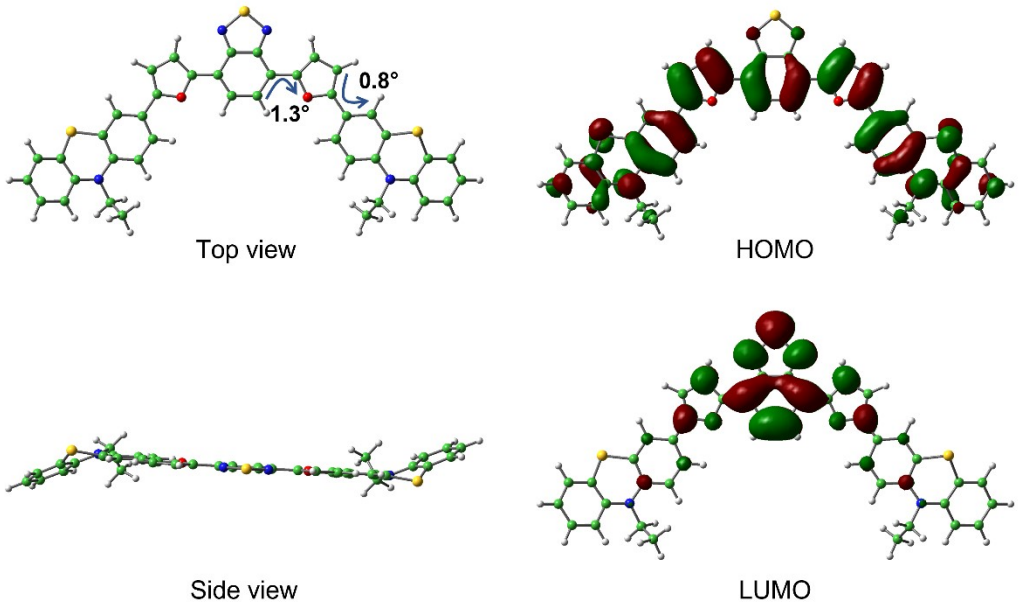

Fig. S4 Optimized structure, the HOMO and the LUMO distributions of the SM37.

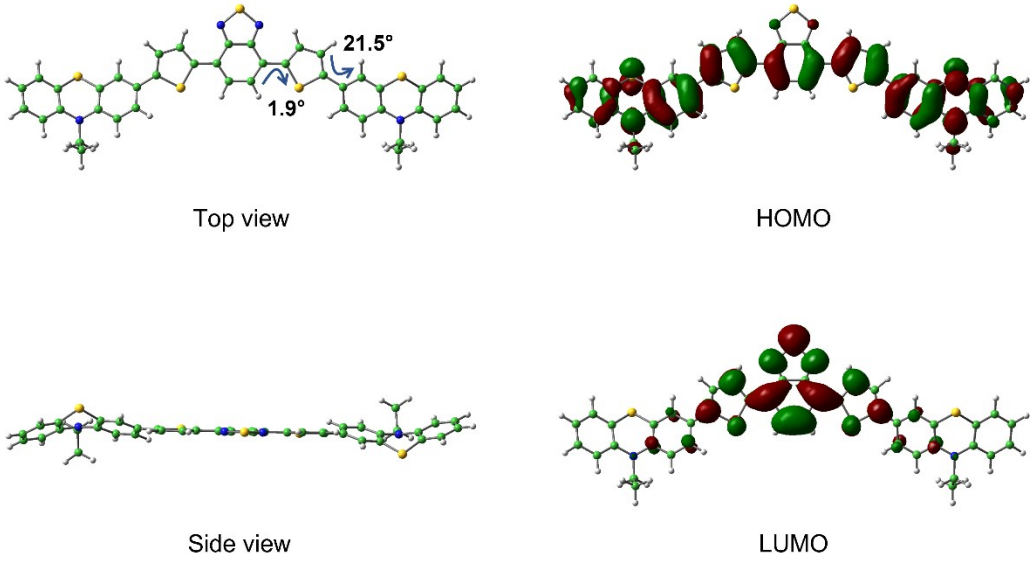

Fig. S5 Optimized structure, the HOMO and the LUMO distributions of the SM38.

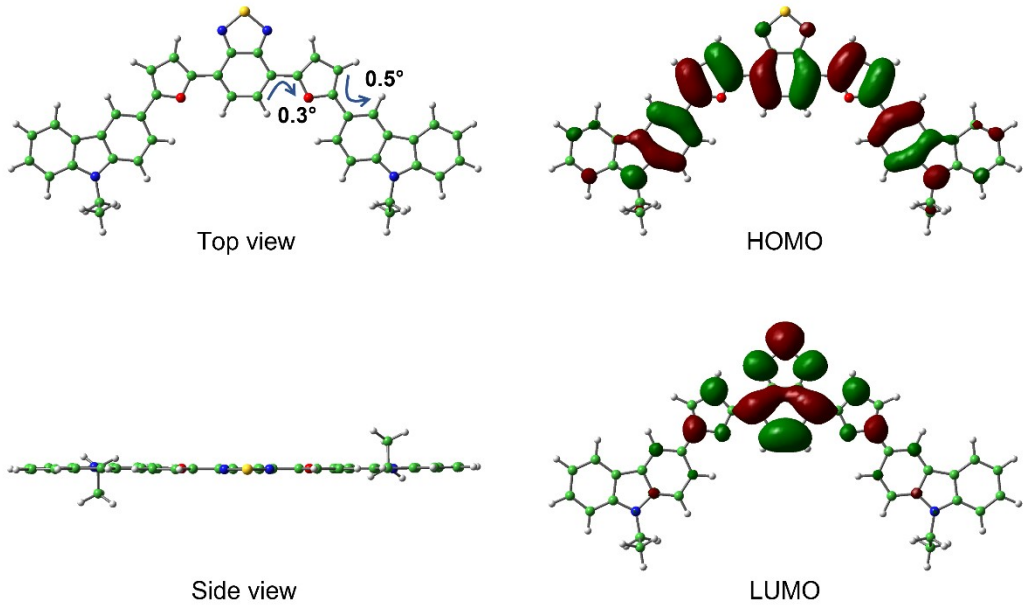

Fig. S6 Optimized structure, the HOMO and the LUMO distributions of the SM39.

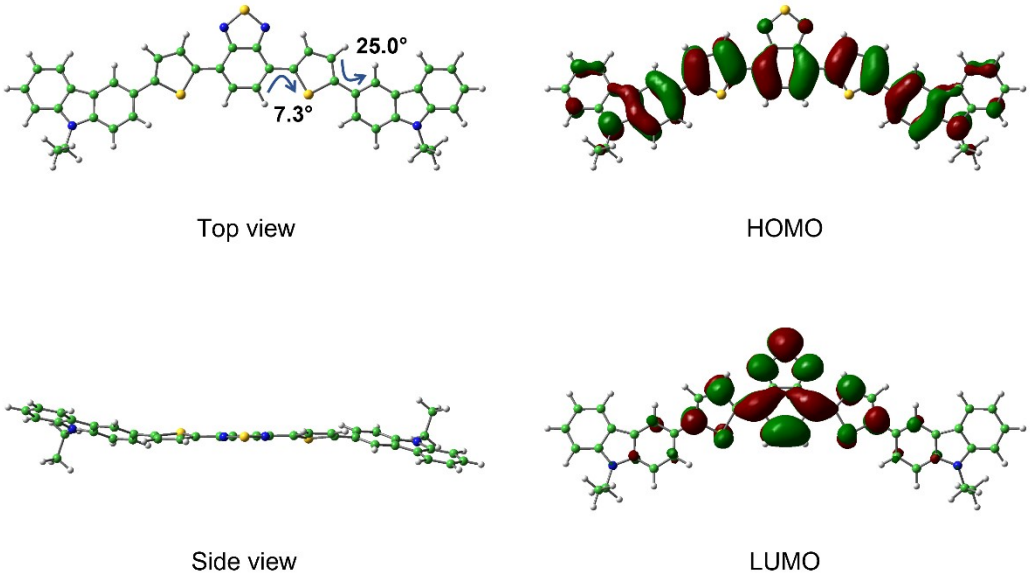

Fig. S7 Optimized structure, the HOMO and the LUMO distributions of the SM40.

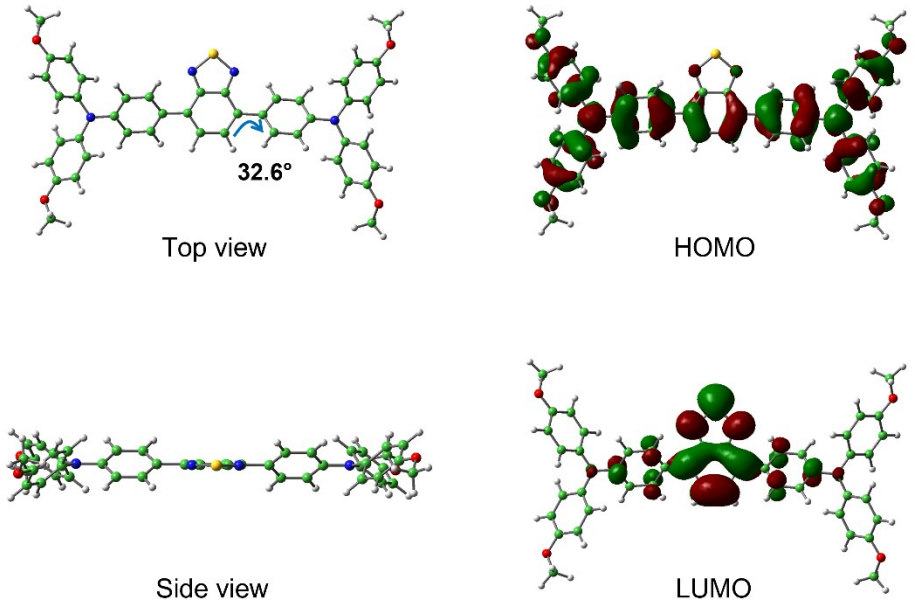

Fig. S8 Optimized structure, the HOMO and the LUMO distributions of the YN1.

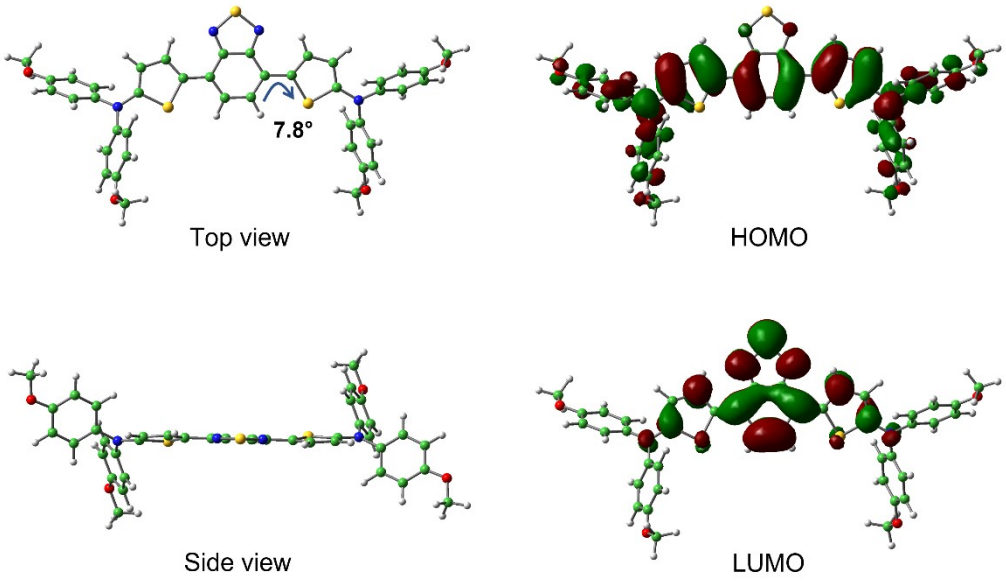

Fig. S9 Optimized structure, the HOMO and the LUMO distributions of the YN1-T.

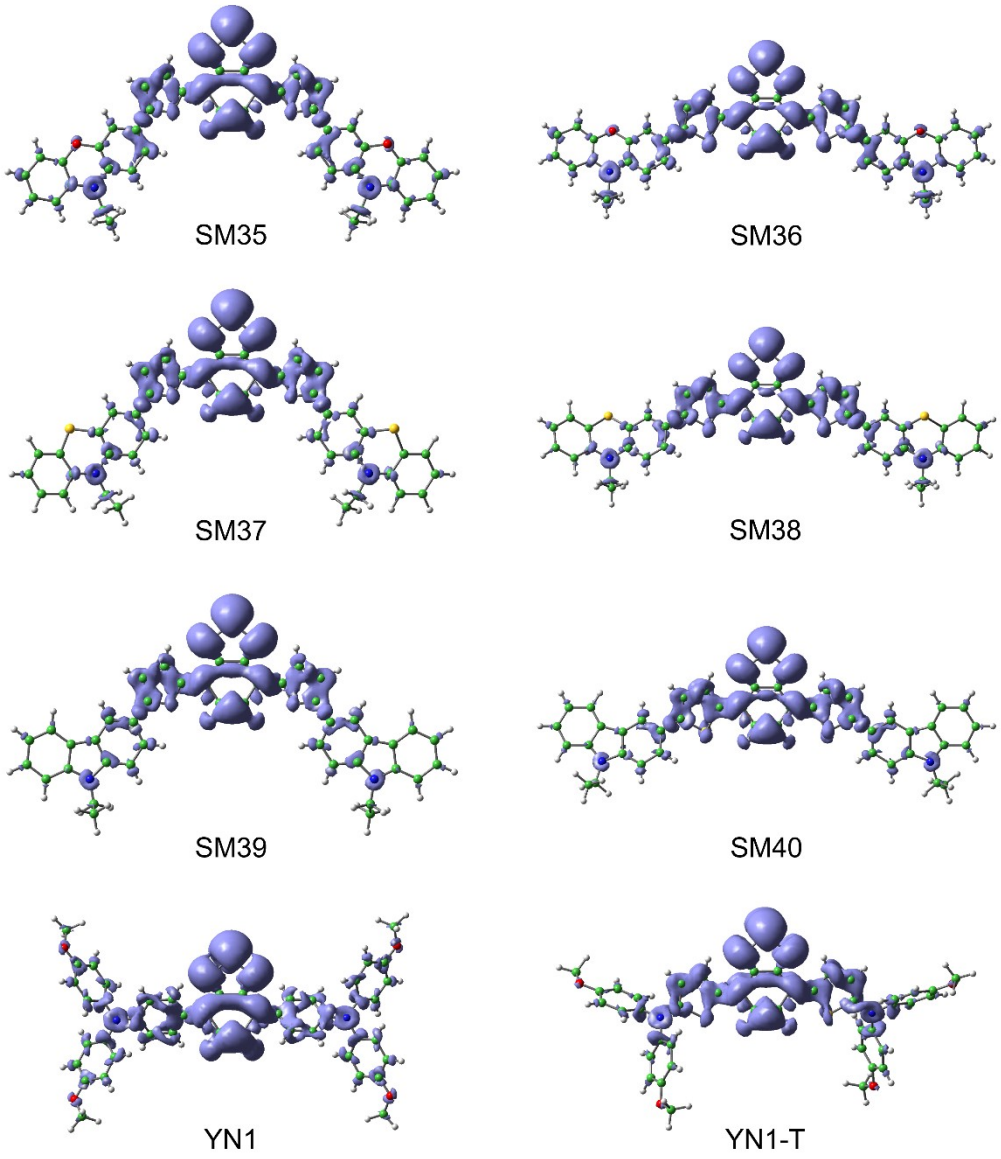

Fig. S10 Charge density difference (CDD) maps of the studied HTMs, and the purple represents where the electrons are increased.

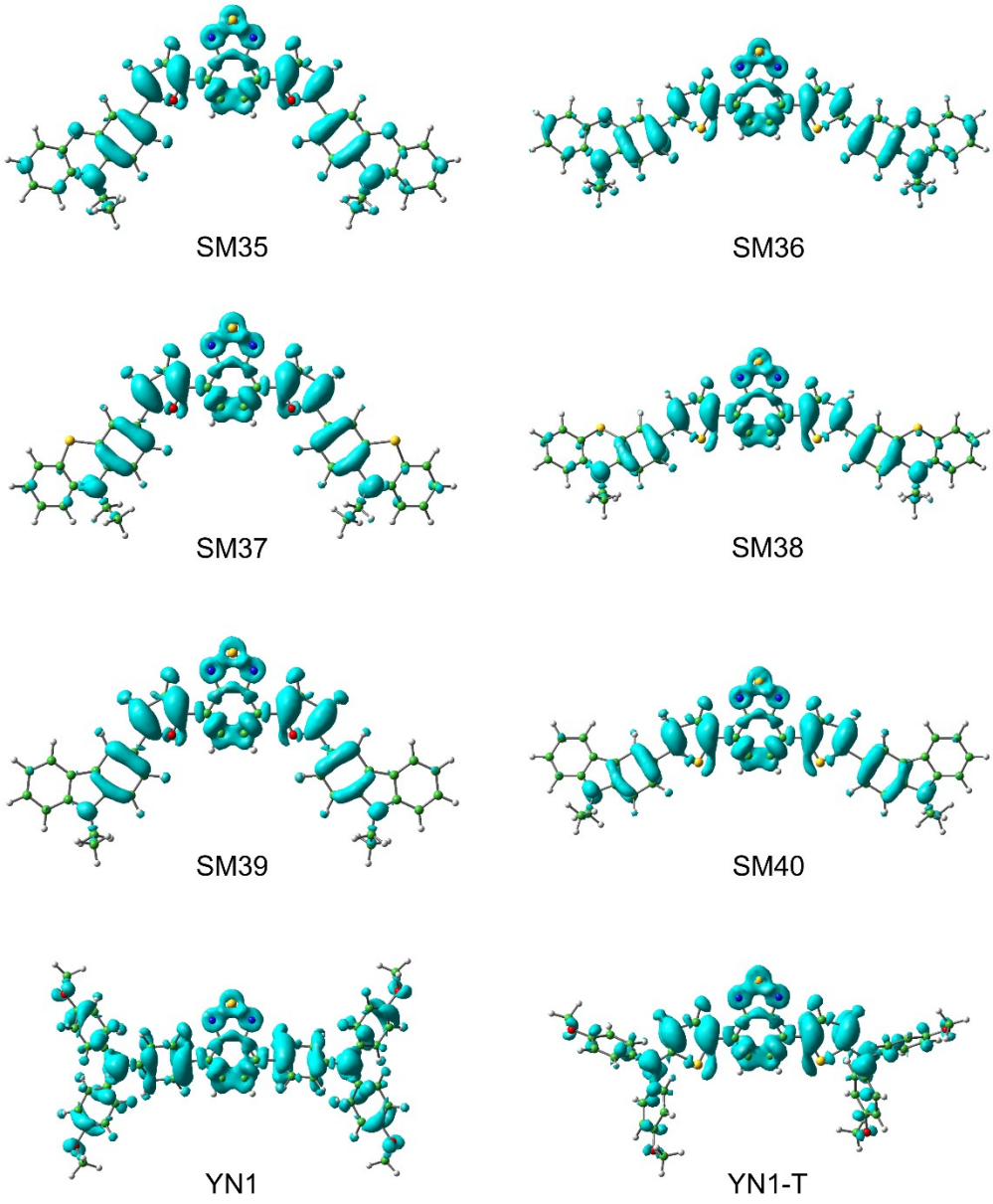

Fig. S11 Charge density difference maps of the studied HTMs, and the blue represents where the electrons are reduced.

Table S3 Hole hopping pathway, centroid to centroid distance (r_i, in Å), hole transfer integral (V_{AB}, in eV), hole hopping rate (κ, in s^{-1}), hole mobility (μ, in $cm^2v^{-1}s^{-1}$), and reorganization energy (λ, in eV) of SM35 in predicted dimeric structures.

HTMs	pathways	r_i	V_{AB}	κ	μ	λ
SM35	1	14.34	3.13×10^{-3}	2.29×10^{10}	1.23×10^{-1}	0.27
	2	14.59	1.05×10^{-3}	2.58×10^{9}		
	3	19.06	1.75×10^{-2}	7.16×10^{11}		
	4	12.84	1.17×10^{-2}	3.20×10^{11}		
	5	12.89	1.76×10^{-2}	7.24×10^{11}		
	6	19.06	1.75×10^{-2}	7.16×10^{11}		
	7	10.66	7.30×10^{-4}	1.25×10^{9}		
	8	10.68	5.58×10^{-4}	7.28×10^{8}		

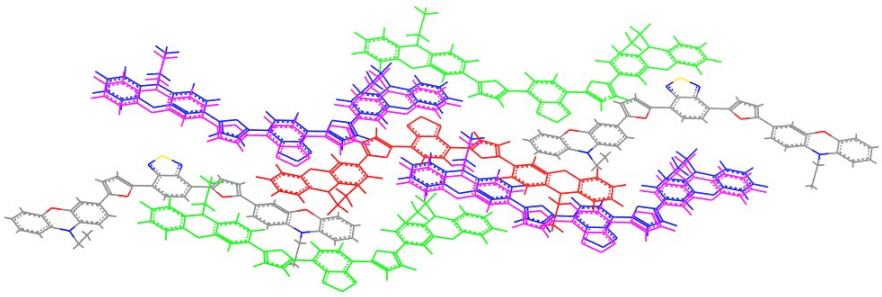

Fig. S12 Selected cluster based on the predicted crystal of SM35 to generate possible hole hopping pathways, where the central molecule is labeled as redness and adjacent molecules are labeled as the other colors.

Table S4 Hole hopping pathway, centroid to centroid distance (r_i, in Å), hole transfer integral (V_{AB}, in eV), hole hopping rate (κ, in s^{-1}), hole mobility (μ, in $cm^2v^{-1}s^{-1}$), and reorganization energy (λ, in eV) of SM36 in predicted dimeric structures.

HTMs	pathways	r_i	V_{AB}	κ	μ	λ
SM36	1	13.66	1.03×10^{-4}	1.97×10^{7}	6.94×10^{-2}	0.29
	2	15.98	7.68×10^{-3}	1.09×10^{11}		
	3	15.98	7.68×10^{-3}	1.09×10^{11}		
	4	24.57	1.25×10^{-3}	2.90×10^{9}		
	5	8.47	2.98×10^{-2}	1.65×10^{12}		
	6	23.24	6.35×10^{-5}	7.48×10^{6}		
	7	9.82	1.83×10^{-3}	6.22×10^{9}		
	8	8.68	1.35×10^{-3}	3.38×10^{9}		

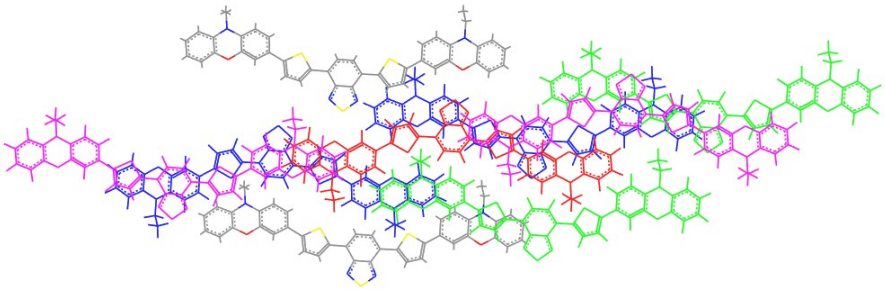

Fig. S13 Selected cluster based on the predicted crystal of SM36 to generate possible hole hopping pathways, where the central molecule is labeled as redness and adjacent molecules are labeled as the other colors.

Table S5 Hole hopping pathway, centroid to centroid distance (r_i, in Å), hole transfer integral (V_{AB}, in eV), hole hopping rate (κ, in s^{-1}), hole mobility (μ, in $cm^2v^{-1}s^{-1}$), and reorganization energy (λ, in eV) of SM37 in predicted dimeric structures.

HTMs	pathways	r_i	V_{AB}	κ	μ	λ
SM37	1	14.72	8.24×10^{-4}	8.01×10^{8}	8.17×10^{-2}	0.33
	2	15.98	2.50×10^{-3}	7.37×10^{9}		
	3	22.56	1.21×10^{-2}	1.73×10^{11}		
	4	8.02	4.16×10^{-2}	2.04×10^{12}		
	5	8.02	4.16×10^{-2}	2.04×10^{12}		
	6	17.78	7.60×10^{-3}	6.81×10^{10}		
	7	11.08	2.90×10^{-3}	9.92×10^{9}		
	8	13.47	6.39×10^{-3}	4.81×10^{10}		

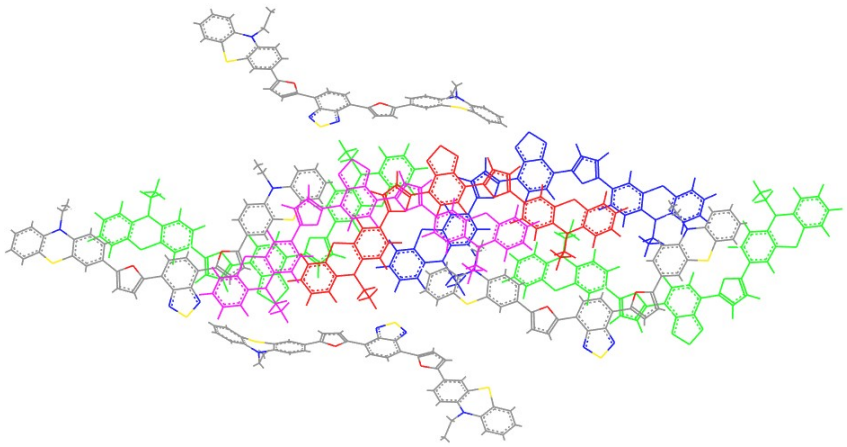

Fig. S14 Selected cluster based on the predicted crystal of SM37 to generate possible hole hopping pathways, where the central molecule is labeled as redness and adjacent molecules are labeled as the other colors.

Table S6 Hole hopping pathway, centroid to centroid distance (r_i, in Å), hole transfer integral (V_{AB}, in eV), hole hopping rate (κ, in s^{-1}), hole mobility (μ, in $cm^2v^{-1}s^{-1}$), and reorganization energy (λ, in eV) of SM38 in predicted dimeric structures.

HTMs	pathways	r_i	V_{AB}	κ	μ	λ
SM38	1	32.21	3.29×10^{-4}	5.87×10^{7}	4.39×10^{-2}	0.40
	2	16.36	8.39×10^{-3}	3.81×10^{10}		
	3	8.85	5.70×10^{-3}	1.76×10^{10}		
	4	8.53	4.37×10^{-2}	1.03×10^{12}		
	5	14.09	2.73×10^{-4}	4.04×10^{7}		
	6	9.54	3.92×10^{-3}	8.33×10^{9}		
	7	16.37	8.39×10^{-3}	3.81×10^{10}		
	8	24.27	8.99×10^{-3}	4.38×10^{10}		

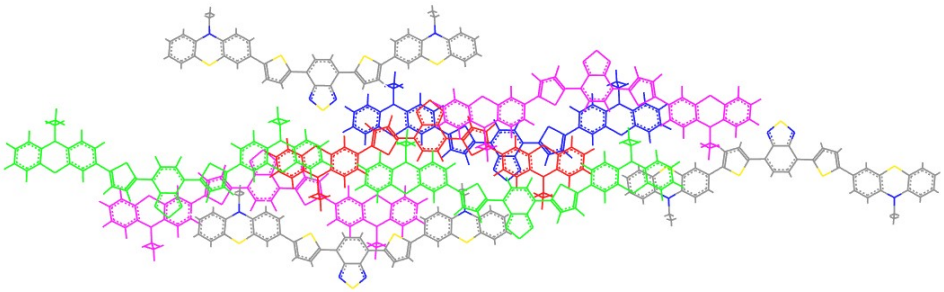

Fig. S15 Selected cluster based on the predicted crystal of SM38 to generate possible hole hopping pathways, where the central molecule is labeled as redness and adjacent molecules are labeled as the other colors.

Table S7 Hole hopping pathway, centroid to centroid distance (r_i, in Å), hole transfer integral (V_{AB}, in eV), hole hopping rate (κ, in s^{-1}), hole mobility (μ, in $cm^2v^{-1}s^{-1}$), and reorganization energy (λ, in eV) of SM39 in predicted dimeric structures.

HTMs	pathways	r_i	V_{AB}	κ	μ	λ
SM39	1	17.72	6.76×10^{-4}	4.31×10^{8}	1.01×10^{-2}	0.35
	2	4.91	2.65×10^{-2}	6.62×10^{11}		
	3	14.87	4.99×10^{-3}	2.35×10^{10}		
	4	4.91	2.65×10^{-2}	6.62×10^{11}		
	5	17.06	2.43×10^{-3}	5.56×10^{9}		
	6	24.38	1.08×10^{-3}	1.10×10^{9}		
	7	9.80	3.74×10^{-3}	1.32×10^{10}		
	8	13.00	1.14×10^{-3}	1.22×10^{9}		

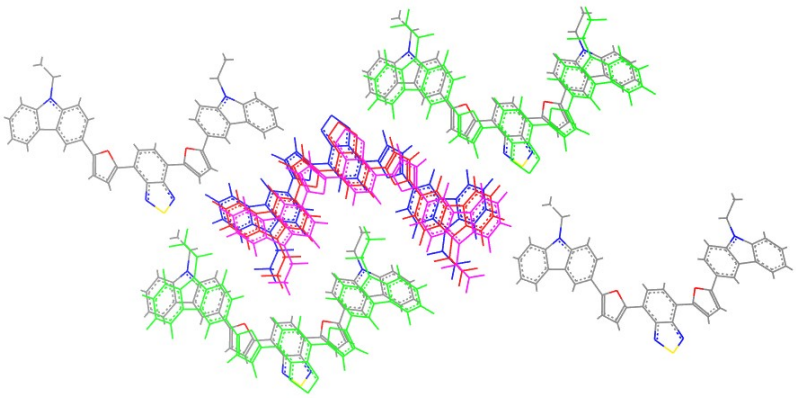

Fig. S16 Selected cluster based on the predicted crystal of SM39 to generate possible hole hopping pathways, where the central molecule is labeled as redness and adjacent molecules are labeled as the other colors.

Table S8 Hole hopping pathway, centroid to centroid distance (r_i, in Å), hole transfer integral (V_{AB}, in eV), hole hopping rate (κ, in s^{-1}), hole mobility (μ, in $cm^2v^{-1}s^{-1}$), and reorganization energy (λ, in eV) of SM40 in predicted dimeric structures.

HTMs	pathways	r_i	V_{AB}	κ	μ	λ
SM40	1	12.11	3.52×10^{-2}	4.84×10^{11}	3.65×10^{-2}	0.43
	2	18.74	9.35×10^{-3}	3.41×10^{10}		
	3	10.93	2.40×10^{-2}	2.25×10^{11}		
	4	21.16	4.75×10^{-3}	8.81×10^{9}		
	5	8.94	5.96×10^{-4}	1.39×10^{8}		
	6	29.76	4.56×10^{-5}	8.12×10^{5}		
	7	7.08	5.42×10^{-2}	1.15×10^{12}		
	8	8.94	5.96×10^{-4}	1.39×10^{8}		

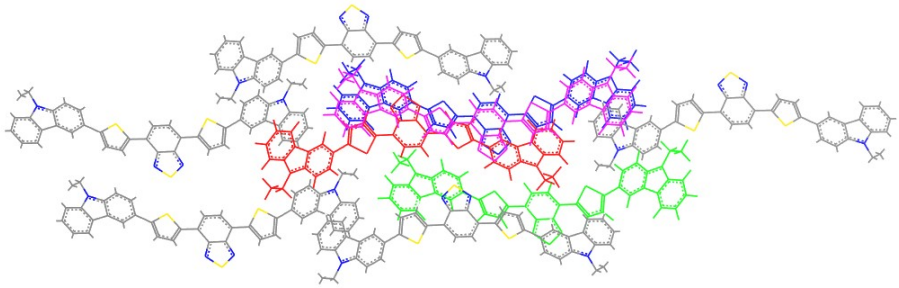

Fig. S17 Selected cluster based on the predicted crystal of SM40 to generate possible hole hopping pathways, where the central molecule is labeled as redness and adjacent molecules are labeled as the other colors.

Table S9 Hole hopping pathway, centroid to centroid distance (r_i, in Å), hole transfer integral (V_{AB}, in eV), hole hopping rate (κ, in s^{-1}), hole mobility (μ, in $cm^2v^{-1}s^{-1}$), and reorganization energy (λ, in eV) of YN1 in predicted dimeric structures.

HTMs	pathways	r_i	V_{AB}	κ	μ	λ
YN1	1	10.03	1.94×10^{-4}	1.58×10^{8}	8.72×10^{-3}	0.22
	2	21.82	1.12×10^{-5}	5.28×10^{5}		
	3	11.61	4.58×10^{-3}	8.83×10^{10}		
	4	21.82	1.15×10^{-5}	5.57×10^{5}		
	5	10.03	1.94×10^{-4}	1.58×10^{8}		
	6	5.96	8.60×10^{-4}	3.11×10^{9}		
	7	8.95	6.59×10^{-3}	1.83×10^{11}		
	8	17.32	8.84×10^{-4}	3.29×10^{9}		

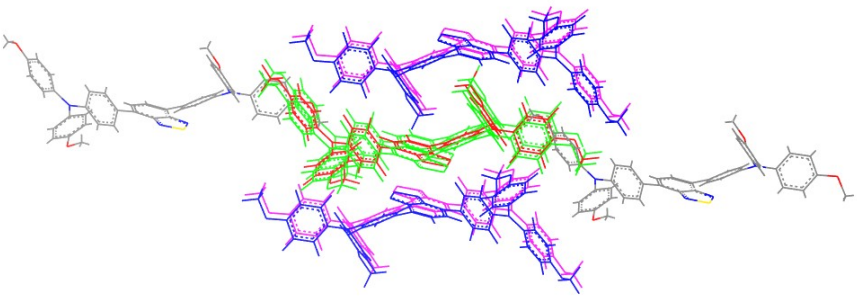

Fig. S18 Selected cluster based on the predicted structure of YN1 to generate possible hole hopping pathways, where the central molecule is labeled as redness and adjacent molecules are labeled as the other colors.

Table S10 Hole hopping pathway, centroid to centroid distances (r_i, Å), hole transfer integral (V_{AB}, in eV), hole hopping rate (κ, in s^{-1}), hole mobility (μ, in $cm^2v^{-1}s^{-1}$), and reorganization energy (λ, in eV) of YN1-T in predicted dimeric structures.

HTMs	pathways	r_i	V_{AB}	κ	μ	λ
YN1-T	1	13.82	5.21×10^{-4}	7.65×10^{7}	1.82×10^{-2}	0.46
	2	7.23	9.87×10^{-4}	2.75×10^{8}		
	3	13.87	1.48×10^{-3}	6.17×10^{8}		
	4	12.94	7.91×10^{-4}	1.76×10^{8}		
	5	13.82	5.21×10^{-4}	7.65×10^{7}		
	6	14.55	1.30×10^{-3}	4.76×10^{8}		
	7	6.90	4.58×10^{-2}	5.91×10^{11}		
	8	12.94	7.94×10^{-4}	1.78×10^{8}		

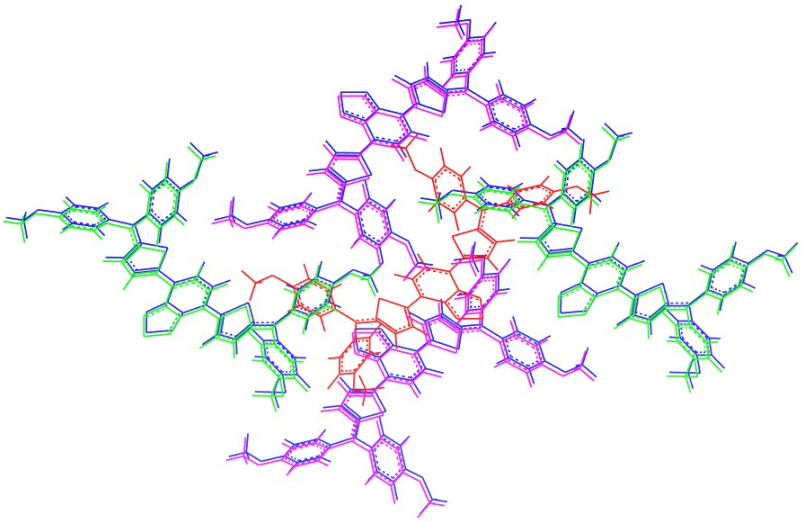

Fig. S19 Selected cluster based on the predicted crystal of YN1-T to generate possible hole hopping pathways, where the central molecule is labeled as redness and adjacent molecules are labeled as the other colors.

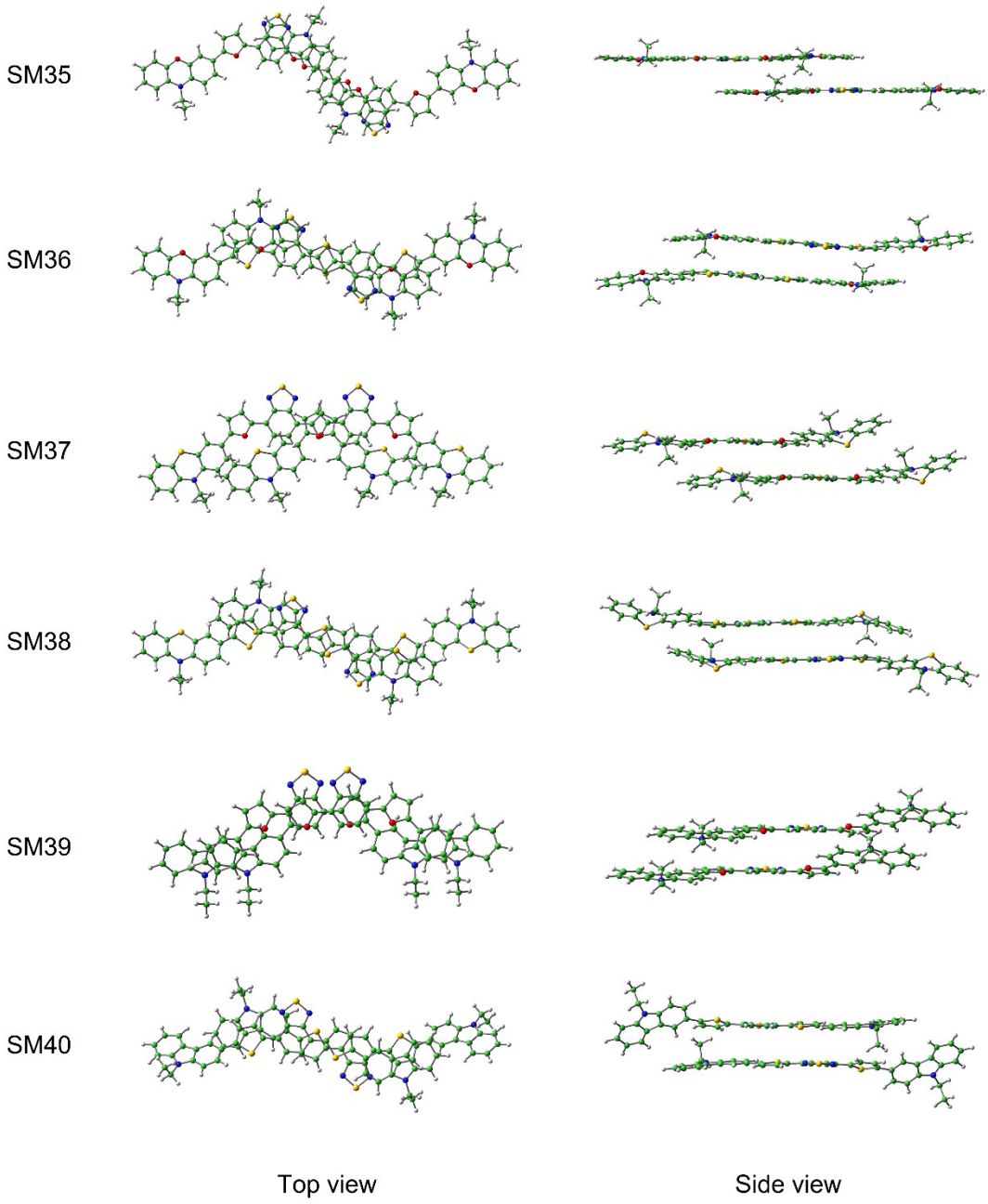

Fig. S20 The dimeric structures of the most main hole transfer pathways.

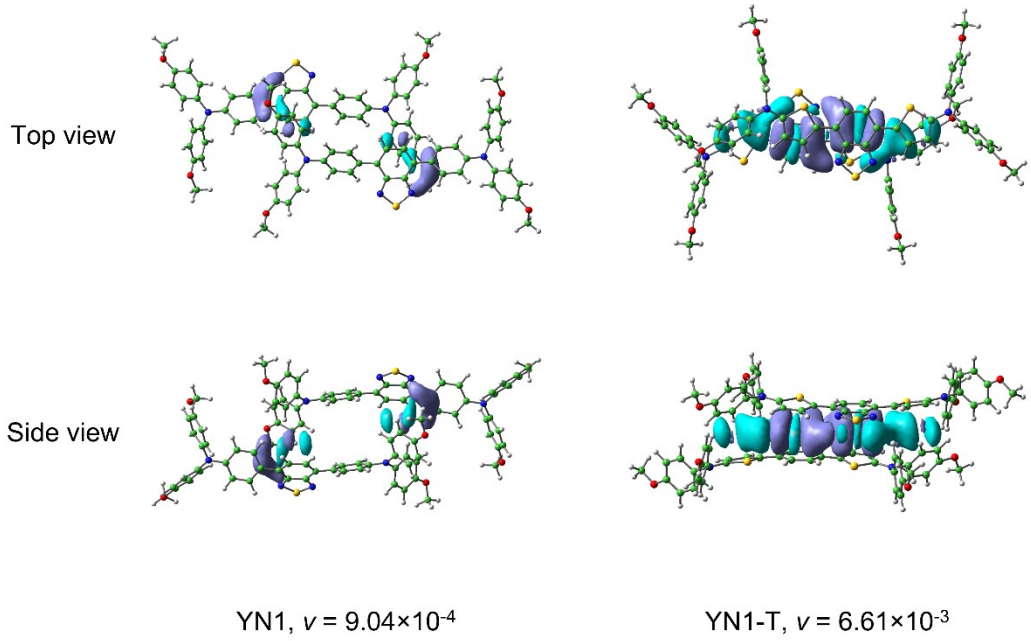

Fig. S21 Isodensity surface plots of the intermolecular HOMO overlaps of the charge transfer channels with the largest hole transfer integrals. The molecular orbital overlap integral values are presented. The isodensity value is set at 5×10^{-6}, and the purple and blue isosurfaces refer to the same and opposite phase overlap, respectively.

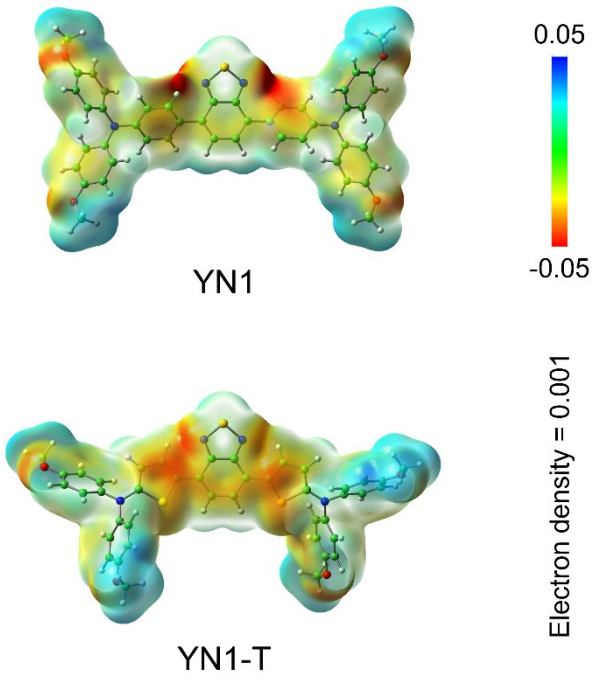

Fig. S22 Electrostatic surface potential mapped onto a surface of total electron density for the YN1 and YN1-T, where regions of negative charge are shown in red and those of positive charge are shown in blue.

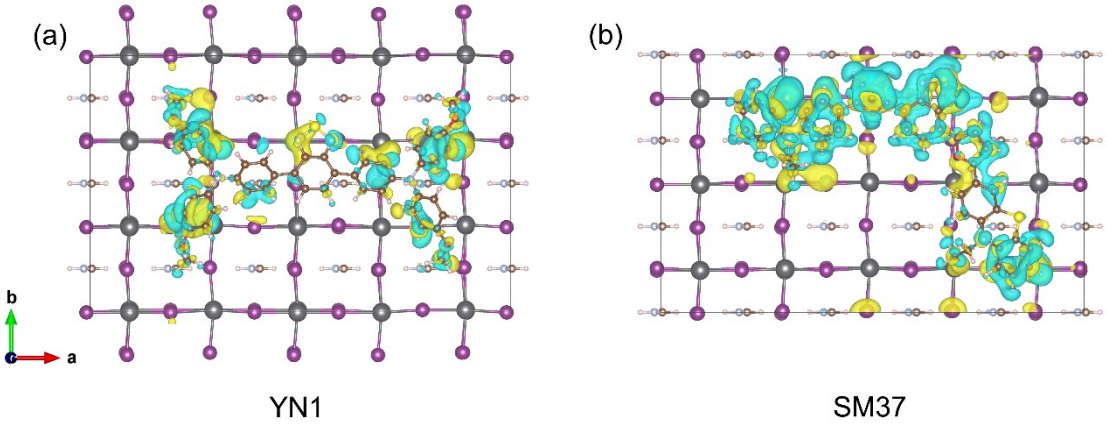

Fig. S23 Calculated charge density difference (CDD) maps of the adsorbed systems of $FAPbI_3$/YN1 (a) and $FAPbI_3$/SM37 (b) from the top view.

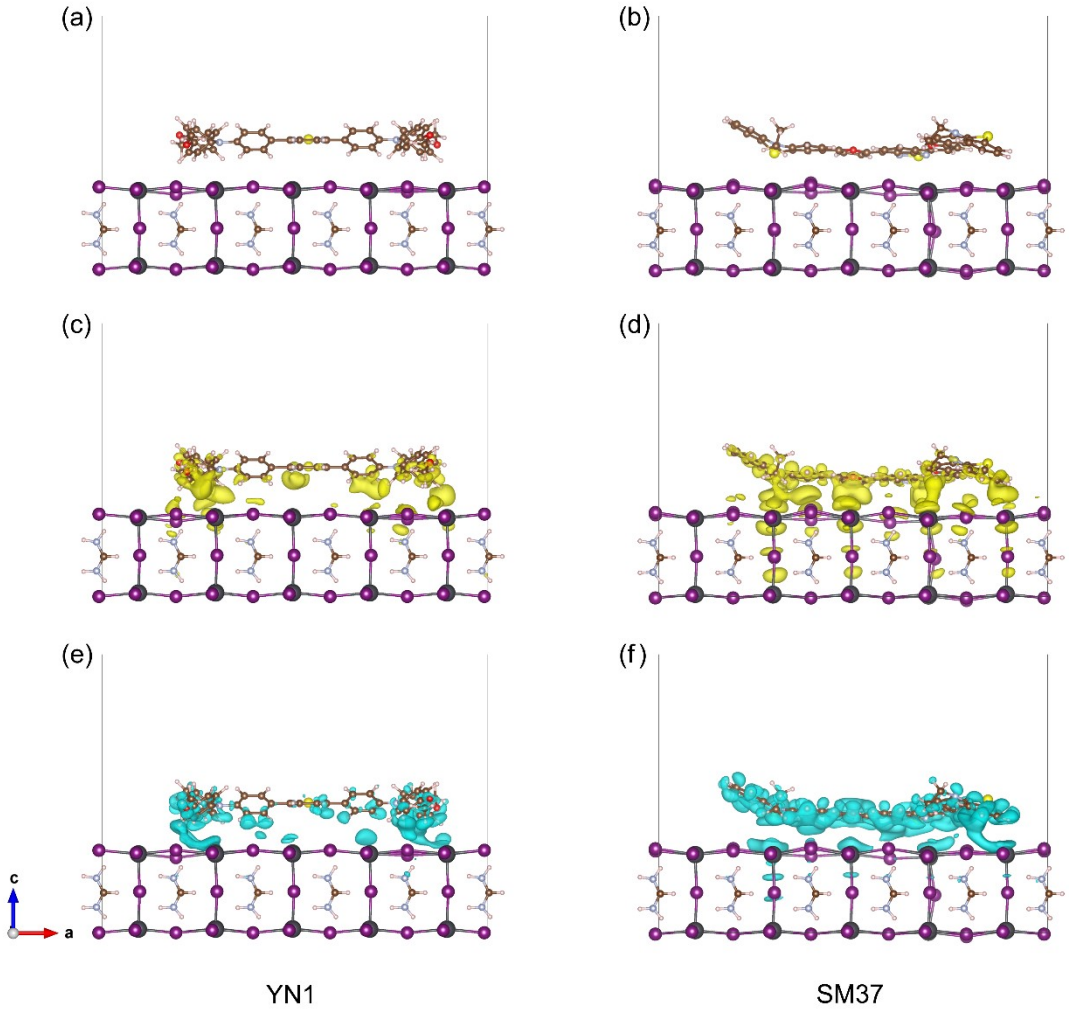

Fig. S24 Adsorbed configurations, charge accumulation and charge depletion for the $FAPbI_3$/YN1 (a, c and e) and $FAPbI_3$/SM37 (b, d and f) systems from the side view.

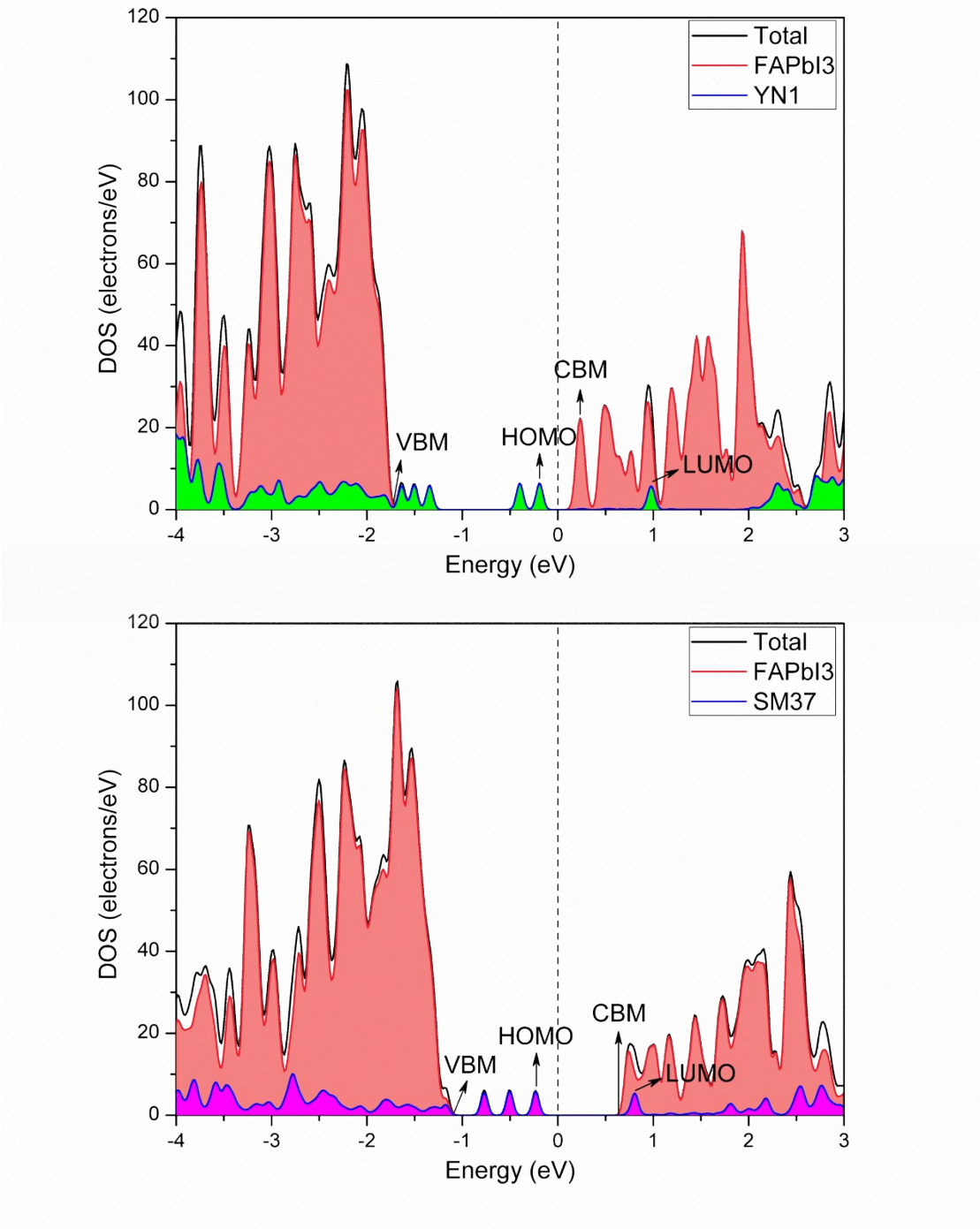

Fig. S25 Total density of states (DOS) and projected DOS (PDOS) for the interfacial systems of $FAPbI_3$/YN1 and $FAPbI_3$/SM37, respectively.